Received: 5 May 2020 | Revised: 20 October 2020 | Accepted: 23 November 2020

DOI: 10.1111/vru.12955

ORIGINAL INVESTIGATION

WILEY

Estimation of planning organ at risk volumes for ocular structures in dogs undergoing three-dimensional image-guided periocular radiotherapy with rigid bite block immobilization

Friederike Wolf[1] | **Carla Rohrer Bley**[1] | **Jürgen Besserer**[1,2,3] | **Valeria Meier**[1,2]

[1] Division of Radiation Oncology, Small Animal Department, Vetsuisse Faculty, University of Zurich, Zurich, Switzerland

[2] Department of Physics, University of Zurich, Zurich, Switzerland

[3] Radiation Oncology, Hirslanden Clinic, Zurich, Switzerland

Correspondence
Valeria Meier, Division of Radiation Oncology, Vetsuisse Faculty, University of Zurich, Winterthurerstrasse 260, CH-8057 Zurich, Switzerland.
Email: vmeier@vetclinics.uzh.ch

Funding sources: This work was supported by the Swiss National Science Foundation (SNSF), grant number: 320030-182490; PI: Carla Rohrer Bley.

Presentation/publication disclosure: Preliminary results of this study were accepted as poster presentation at the ESVONC congress in May 2020 (cancelled due to COVID-19 pandemic).

EQUATOR network disclosure: The STROBE-Vet checklist was used for preparation of this manuscript

Abstract

Planning organ at risk volume (PRV) estimates have been reported as methods for sparing organs at risk (OARs) during radiation therapy, especially for hypofractioned and/or dose-escalated protocols. The objectives of this retrospective, analytical, observational study were to evaluate peri-ocular OAR shifts and derive PRVs in a sample of dogs undergoing radiation therapy for periocular tumors. Inclusion criteria were as follows: dogs irradiated for periocular tumors, with 3D-image-guidance and at least four cone-beam CTs (CBCTs) used for position verification, and positioning in a rigid bite block immobilization device. Peri-ocular OARs were contoured on each CBCT and the systematic and random error of the shifts in relation to the planning CT position computed. The formula $1.3\times\Sigma+0.5\times\sigma$ was used to generate a PRV of each OAR in the dorsoventral, mediolateral, and craniocaudal axis. A total of 30 dogs were sampled, with 450 OARs contoured, and 2145 shifts assessed. The PRV expansion was qualitatively different for each organ (1-4 mm for the dorsoventral and 1-2 mm for the mediolateral and craniocaudal axes). Maximal PRV expansion was ≤4 mm and directional for the majority; most pronounced for corneas and retinas. Findings from the current study may help improve awareness of and minimization of radiation dose in peri-ocular OARs for future canine patients. Because some OARs were difficult to visualize on CBCTs and/ or to delineate on the planning CT, authors recommend that PRV estimates be institution-specific and applied with caution.

KEYWORDS
canine, eye, PRV, sinonasal, toxicity

1 | INTRODUCTION

The planning organ at risk volume (PRV) gained more attention in the age of newer radiation techniques aiming at higher total doses or larger dose per fraction and thereby increasing the probability of damaging organs at risk (OARs). An OAR or critical normal structure is normal tissue whose radiation sensitivity can markedly influence treatment planning. It often lies in the very close vicinity of target volumes or even within the high dose area. OARs are often mobile/ deformable structures. In addition, they are subject to similar setup inaccuracies as target volumes during radiation therapy (RT). To compensate for these

Abbreviations: CBCT, cone-beam computed tomography; CTV, clinical target volume; GTV, gross tumor volume; IMRT, intensity-modulated radiation therapy; kV, kilovolt; OAR, organ at risk; PRV, planning organ at risk volume; PTV, planning target volume; RT, radiation therapy

geometrical variations, a margin expansion is added to OARs, resulting in the respective PRV.[1] The PRV enables avoiding functional damage in the OAR as it limits dose to specific, tolerated levels during the treatment planning process. For sinonasal tumors in dogs, multiple PRVs can be constructed for (peri-)ocular OARs such as globe, lens, as well as optic nerve, chiasm, and lacrimal glands.

Before the age of newer radiation techniques in veterinary medicine, moderate to severe damage to ocular structures was common, when treating sinonasal tumors in dogs, and could not be avoided technically. This resulted in painful toxicities, often leading to (unilateral) loss of vision, enucleation and other pathological changes.[2] Nowadays, with intensity-modulated radiation therapy (IMRT), selective sparing of OARs is technically more feasible.[3,4] In general, ocular OARs are not strongly subject to large position changes during RT, but ocular globes can rotate depending on anesthetic status.[5] In dogs and cats, a lens PRV has been calculated but it is not currently known how other (peri-)ocular structures move during a course of RT.[6]

Objectives of the current study were to evaluate translational shifts of (peri-)ocular OARs during a course of RT with the goal of defining PRVs in dogs for each (peri-)ocular structure in each axis. To meet this goal, the formula derived by van Herk was used to calculate random and systematic errors of shifts detected by on-board imaging from dogs treated for periocular tumors.[7,8]

2 | METHODS

2.1 | Case selection

The study was a retrospective, analytical, observational design. Computed tomography (CT) datasets of client-owned dogs formerly treated with RT for a neoplasia in the proximity of the eye at the Vetsuisse Faculty of the University of Zurich during the period of January 2016 and December 2019 were considered for inclusion. Sample size for the study was based on convenience sampling. Datasets were included by a board-certified veterinary radiation oncologist (V.M., Diplomate of the American College of Veterinary Radiology [Radiation Oncology], DACVR [RO]) if all OARs were included in CT images, if the institution's rigid immobilization device had been used and the dog's treatment position verified with at least four cone-beam CTs (CBCTs) during a course of treatment. Information regarding signalment, tumor type and location was collected from medical records. All owners had signed the hospital's informed consent form stating their pet's data could be published anonymously.

2.2 | Computed tomography and positioning verification

As part of the inclusion criteria for the study, all dogs had undergone a planning CT with the institution's rigid patient positioning system under general anesthesia for previous treatment. Magnetic resonance imaging was not available. The positioning system consisted of an individually shaped vacuum cushion (BlueBag BodyFix, Elekta AB, Stockholm, Sweden) supporting the thorax/ front legs and a custom-made bite block (President The Original, Putty Soft, Coltène, Whaledent AG, Altstaetten, Switzerland) supporting the upper jaw fixed on a polycarbonate tray on the treatment couch. Before each treatment, the patient position was verified using daily 2D kilovolt (kV) orthogonal digitally reconstructed radiographs and occasional kV-cone-beam CT (CBCT). The treatment patient positioning was the same as for the planning CT. For a 10-fraction-protocol, CBCTs were performed before the 1./5./6./10. fraction as by our institution's guidelines (except in case of marked discrepancy between digitally reconstructed radiograph and CBCT). If a dog showed marked pitch or roll (which cannot be corrected with our 4-degree of freedom treatment table), it was repositioned and imaging repeated. Definition of marked pitch/roll was based on the attending radiation oncologist's judgement, at our institution interpreted as visible head nodding/movement when quick back and forth switching of superimposed CT to CBCT images was performed. If corrections of yaw, lateral, vertical or craniocaudal displacement were noted, this was corrected online, the information used to correct the table position before starting treatment (accepted treatment position match) and used in the present contouring study. The final treatment positions were confirmed by an experienced radiation therapist and/or veterinary radiation oncologist. Details regarding CT/CBCT settings were collected.

2.3 | Contouring of organs at risk on planning computed tomography

At the time of treatment planning for prior treatment of included dogs, the planning CT images were imported into the External Beam Planning system (Eclipse™ Planning system, version 10.0.28 or 15.1.25; Varian Oncology Systems, Palo Alto, California, USA). The contouring workspace was used to delineate (peri-)ocular OARs on each planning CT. All OARs were converted to high resolution segment and the OAR contouring guidelines for (a) ocular globe, (b) ocular lens, (c) optic nerve, (d) optic chiasm, (e) retina (defined as "retina-choroid-sclera complex"), and (f) lacrimal gland were used as previously described.[9] The lens was contoured as hyperattenuating structure on the precontrast CT images. The lacrimal glands were contoured on post-contrast images along the dorsolateral aspect of the globe deep to the orbital ligament.[10] To facilitate delineation of the "retina-choroid-sclera complex," a 1 mm margin was contoured around the ocular globe, the crop tool was used to crop the eye from the retina and the eraser tool was used to erase by hand where the structure entered the cornea. (g) The cornea – located rostral to the anterior chamber – was contoured similarly except that the crop tool was also used to remove the part overlapping with the retina.[11] The distinction between the end of the retina and the start of the cornea was not clearly visible and therefore a subjective choice based on the presumed location of the *iridocorneal angle* (with aid of the medial and lateral aspect of the lens) according to an anatomical textbook.[11] (h) The accessory lacrimal glands were contoured on post-contrast images located at the base of the vertical cartilage of the third eyelid.[10] The volume of each periocular and ocular structure was documented in mm^3 using the measure 3D volume fea-

ture in the external beam planning system. All of the contouring was newly performed for this study by a veterinarian (F.W.), checked by a board-certified veterinary radiation oncologist (V.M., DACVR[RO]), and a consensus was reached.

2.4 | Contouring of OARs on CBCTs for PRV estimation

We used the online registration of each CBCT to the planning CT with manual, computer-based adjustment of the dog's actual position to the aspired treatment position (with the planning CT as reference) in the mediolateral, craniocaudal, and dorsoventral axis – as performed for previous treatment (ie, no new, standardized registration was performed). The observers were not aware of the shifts in position, as all contours were delineated on the CBCT images. Some OARs were difficult to address on the CBCT or were of different volume if contoured from scratch (even if a change in volume of the organ seemed very unlikely). This was due to a lack of contrast agent administration and/ or poorer image quality (in comparison to the diagnostic images). We therefore created helper structures from the planning CT ocular OARs to facilitate contouring them on the CBCTs: (a) Ocular globe: The first helper structure consisted of the volume of the ocular globe copied from the planning CT (Eye_{CBCT}). This was repeated to create one helper structure for each CBCT respectively (eg, Eye_{CBCT1}, Eye_{CBCT2}, Eye_{CBCT3}, Eye_{CBCT4}). The transform structure tool was used to shift (translational) this volume to match the appropriate position in the co-registered CBCT. (b) Lens: The helper structure for the lens consisted of the Eye_{CBCT} minus the lens using the crop structure tool ($LensHelper_{CBCT}$). After adjusting the helper structure (eye minus lens) to match the lens, we contoured the lens on the CBCT by using the brush tool with the extra function of avoiding drawing over the helper structure. A helper structure was used to facilitate contouring and avoid underestimating the lens volume because the CBCT lens structures were consistently smaller. This was most likely owed to inferior (CB-)CT quality. (c) Optic nerves: The optic nerves were newly contoured on each CBCT from the posterior aspect of the ocular globe to the optic canal in the sphenoid bone. Because only the first third of the optic nerve was visible on the CBCT after leaving the posterior aspect of the ocular globe, we used the planning CT optic nerve as guideline to create an optic nerve of similar size. (d) Optic chiasm: The optic chiasm of the planning CT was copied for each CBCT and adjusted for minimal changes of head position with the presphenoid bone as a matching point. (e) Retinas and (g) corneas: Both structures of the planning CT were duplicated for each CBCT and adapted to the respective Eye_{CBCT} structure with help of the transform structure tool as described above. Again, the lens served as a guide for aligning both structures to show the presumed location of the iridocorneal angle. (f) Lacrimal glands: The lacrimal glands were not well visible on unenhanced CBCT images (as described previously[10]) and were therefore duplicated and moved to the presumed CBCT position along the dorsolateral aspect of the eye underneath the orbital ligament with the transform structure tool. (h) Accessory lacrimal glands: Similarly, the accessory lacrimal glands were not visible on CBCTs.[10] A helper structure consisting of the accessory lacrimal gland and part of the bone in immediate proximity (using the segmentation wizard for bone and choosing a field of view that included only the bone nearby) was created. This helper structure was then adjusted to the CBCT with the transform structure tool. The final CBCT accessory lacrimal gland structure resulted from removal of the bone from the helper structure. The volumes of all new CBCT OARs (excluding the ones contoured with a helper structure or created with duplication) were measured in mm^3. The number of CBCTs per dog was documented, as well as the number of fractions, total dose, and dose per fraction.

2.5 | Establishing estimated planning organs at risk volume

Due to online registration, the same coordination system was used for OAR on the CBCT and planning CT. To assess the shifts, we therefore retrieved the coordinates (in the dorsoventral, mediolateral, and craniocaudal axis) of each ocular CBCT OAR on the planning CT using the tool "move to isocenter of the structure" in the contouring workspace. Those coordinates where then subtracted from the coordinates from the same (reference) structure of the planning CT to reveal the shift in millimeters (mm).

The formula $1.3\times\Sigma + 0.5\times\sigma$ for the calculation of the safety margin proposed by van Herk et al. was used to evaluate the shifts of the OAR on CBCTs compared to the planning CT position in the dorsoventral, mediolateral, and craniocaudal axis.[7,8] The Σ represents the systematic error and was calculated as the standard deviation of the mean shifts of all dogs for all available CBCTs. The σ represents the random error and was calculated as the quadratic summation of the standard deviation of the shifts of each individual dog over the course of treatment. Hence, the formula generated an estimated PRV of each OAR in each axis separately for our population of dogs.

2.6 | Statistical analysis

Statistical tests were selected and performed by two observers with mathematical and clinical trial expertise. Data were coded in a spreadsheet (Microsoft®, Excel for Mac, Version 16.43, Microsoft, Redmond, WA 98052-6399 USA) and analyzed with a commercial statistical software package (IBM® SPSS® Statistics, Version 24, IBM Corp., Armonk, New York). A graphical assessment and Shapiro-Wilk normality test was performed on all data and mean ± standard deviation (SD) or median and interquartile range (IQR) was reported, as appropriate. Descriptive statistics such as mean and SD (for continuous variables such as weight) and median and interquartile range for non-normally distributed continuous variables (age, OARs) and absolute and relative frequencies for discrete variables (sex, CBCTs) were computed by an experienced veterinary radiation oncologist (C.R.B., DACVR[RO]), formulas including systematic and random errors by an experienced medical physicist (J.B.).

3 | RESULTS

3.1 | Case characteristics

A total of 30 dogs were included in this study. The dogs presented with different sinonasal (n = 23), maxillary (n = 3), and brain (n = 4, olfactory bulb) neoplasia. Median age was 10.2 years (IQR 2.9, range 5.6-15.4 years). There were 12 neutered male, nine spayed female, five intact male, and four intact female dogs. Both mixed breed and purebred dogs were represented with most dogs (29/30) being mesocephalic/dolichocephalic dogs and one dog (1/30) being brachycephalic. Body weight ranged from 3.3 to 69.0 kg, with a mean of 24.6 (±14.6) kg.

3.2 | Computed tomography and positioning verification

A pre- and postcontrast standard CT scan of each dog was performed with the same 16-slice CT scanner (Brilliance CT, Philips Health Care Ltd, Best, the Netherlands) as previously described.[12] Technical parameters for the CT scans are available in Supplementary file 1. Postcontrast series were performed after intravenous administration of 2 ml/kg of contrast medium (Accupaque™, Iohexol, 350 mg I/mL, osmality of 780mOsmol/kg, GE Healthcare AG, Switzerland) using a power injector (Accutron CT-D, Med Tron, AG, Germany). For treatment, a linear accelerator (Varian Clinac iX, Varian Medical Systems, Palo Alto, USA) with a four degrees-of-freedom couch was used. All CBCTs were performed with the on-board imaging system (Varian On-Board Imager®, Varian, Palo Alto, USA). Prior to treatment delivery, a kV-CBCT was acquired and matched by a certified and experienced radiation therapist. CBCT settings used in 25 cases were 100 kV (x-ray tube voltage), 20 mA (x-ray tube current), 144mAs (exposure), 17.2 cm scan length and full fan mode; a full 360° acquisition was used at 180°/min. The maximum diameter for reconstruction was 250 mm; 512 × 512 pixels and a resolution of 0.488 mm. The CBCT settings in five newer cases were 100 kV (x-ray tube voltage), 80 mA (x-ray tube current), 1310mAs (exposure), 18 cm scan length and full fan filter; a full 360 acquisition was used at 180/min. The maximum diameter for reconstruction was 100 mm; 512 × 512 pixels and a resolution of 0.195 mm. Quality assurance of the on-board imager was performed as required by institutional and federal guidelines.[13] The tests ensure that the geometrical error of the CBCT acquisition and reconstruction in addition to the error of the couch shift is within a 1 mm tolerance.

All CBCT images were automatically imported into the treatment planning system (Eclipse version 10.0.28 or 15.1.25, Varian Oncology Systems, Palo Alto, USA) at their initial setup position, with 2 mm slice spacing. The number of CBCTs performed and contoured per patient was as follows: 4 (18 dogs), 5 (7 dogs), 6 (2 dogs), and 7, 8, or 9 CBCTs in one dog each with a median of 4 (IQR 1, range 4–9). The median number of fractions, dose per fraction and total dose were 10 (IQR 0, range 10–18), 4.2 Gy (IQR 0.3, range 3–4.83 Gy), and 42 Gy (IQR 6.3, range 30–54 Gy), respectively, administered with 6MV photons.

3.3 | Ocular organs at risk on planning computed tomography and cone-beam computed tomography

A total of 450 OARs were contoured on the planning CTs and 2145 on CBCTs. An example case of a planning CT is shown in Figure 1A,B. The volume of the ocular OARs is depicted in the Supporting Information 2 (except for CBCT structures where a template helper structure with the same OAR size as in the planning CT was used). Optic chiasm volume was zero because export from the treatment planning system led to very small volumes (<0.004 mm^3) that equaled zero when automatic mathematical rounding was used.

3.4 | Establishing estimated planning organs at risk volume

A total of 2145 shifts were assessed. PRV expansion was different for each organ and each axis with a range of 0.097-3.817 mm. An example case is shown in Figure 2A,B. Since non-isotropic expansion is possible with contouring systems today and is more reasonable in OAR with directional shifts, a tailored PRV expansion can be chosen based on the calculations as presented in Table 1. For easier clinical implementation, a rounded number per organ is shown in Table 2.

4 | DISCUSSION

This study aimed at developing a PRV estimation for ocular structures in dogs with use of our rigid positioning system. Almost two decades ago, McKenzie et al. established a PRV formula to account for geometric uncertainties (random and systematic error) during the RT process. This ensures that – despite geometric uncertainty – the dose in the PRV as shown in the dose-volume-histogram is a better estimate of the dose received by the OAR over the whole course of treatment compared to the dose in the OAR volume alone. The systematic uncertainties were rather large at that time because positioning was based on lasers matched on the surface of the (prostate) cancer patient and no daily image-guidance was performed.[7] Nevertheless, the formula originally derived by van Herk is still in use today.[6,8,14,15]

At present, positioning errors can be corrected before each fraction in human and more and more also in veterinary radiation facilities due to frequent or even daily image-guidance with orthogonal radiographs or CT. Subsequently, CBCT-guided RT and better positioning devices led to a decrease in the systematic error and therefore smaller PTV and PRV expansions.[15–23] Smaller PTV expansions, advanced equipment and treatment techniques led to conformal avoidance with the possibility to use dose-escalated and/or more hypofractionated radiation protocols in sinonasal and other tumors in dogs.[4,9,24–28] Intensity-modulated and volumetric-modulated arc RT allows the planner to actively choose how much dose is deposited in a certain region. A steep dose fall-off can be aspired close to an OAR with serial architecture while allowing distribution of a lower dose to a larger amount of non-critical normal tissue. Thus, more careful sculpting of (high) radiation

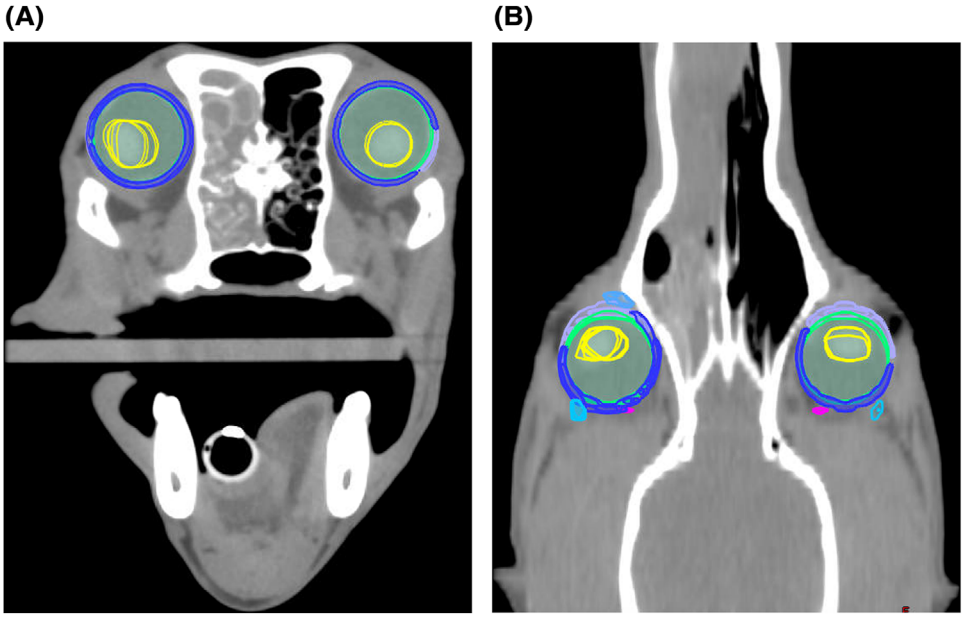

FIGURE 1 A, Transverse and B, dorsal plane CT image of the head as imported into the treatment planning system (slice thickness 2 mm, soft tissue algorithm, 450/140 window width/level, sternal recumbency) at the level of the lenses (yellow) and eyes (green) showing the different positions of the OARs from the planning CT and four CBCTs. Also seen: retina-sclera-complex (dark blue), cornea (violet), accessory and lacrimal glands (light blue), optic nerve (pink) [Color figure can be viewed at wileyonlinelibrary.com]

TABLE 1 Planning organ at risk volume expansion margins of ocular organs at risk in sampled dogs

OARs for all dogs (N = 30)	Dorsoventral PRV expansion [mm]	Mediolateral PRV expansion [mm]	Craniocaudal PRV expansion [mm]
Ocular globe left	0.886	1.049	1.321
Ocular globe right	0.780	0.780	1.224
Lens left	1.493	1.342	1.726
Lens right	1.763	1.331	1.679
Optic nerve left	2.409	1.429	1.452
Optic nerve right	1.660	1.537	1.156
Optic chiasm	0.665	1.085	0.895
Retina left	1.416	1.141	1.265
Retina right	2.215	0.915	1.248
Cornea left	3.069	2.036	2.118
Cornea right	3.817	2.138	2.076
Lacrimal gland left	0.690	0.862	0.097
Lacrimal gland right	1.006	0.957	0.154
Accessory lacrimal gland left	1.032	1.256	0.409
Accessory lacrimal gland right	0.707	1.087	0.471

OARs: organs at risk, PRV: planning organ at risk volume.

dose around nearby OARs or PRV is of even greater importance today. This is especially true for irradiation of sinonasal tumors to avoid possibly debilitating late toxicity.[2] As far as we know, only a PRV of the lens but no other ocular or periocular structures exists for dogs.[6]

The present work described OAR contouring guidelines and a PRV estimation for (peri-)ocular OARs when positioned in a custom-made bite-block and mattress and treated with 3D-image-guided RT and use of a 4-degree-of-freedom treatment table. Our PRV was based on the

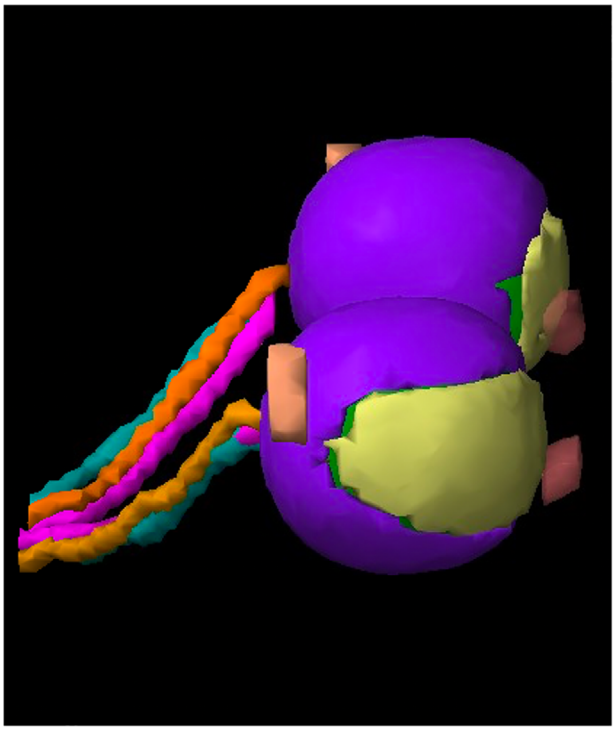

FIGURE 2 Three-dimensional-image of the right (on top) and left eye (at the bottom) from the planning CT with ocular globes (green), corneas (yellow), retina-sclera-complex (purple), accessory lacrimal glands (light pink), lacrimal glands (light orange), and optic nerves (orange). Two additional optic nerve contours from two CBCTs on each side are shown in pink and turquoise to demonstrate small positional shifts [Color figure can be viewed at wileyonlinelibrary.com]

TABLE 2 Estimated ocular planning organ at risk volume expansion margins for clinical use

OARs for all dogs (N = 30)	Dorsoventral PRV expansion [mm]	Mediolateral PRV expansion [mm]	Craniocaudal PRV expansion [mm]
Ocular globe	1	1	1-2
Lens	2	1-2	2
Optic nerve	2-3	2	1-2
Optic chiasm	1	1	1
Retina	2-3	1	1-2
Cornea	3-4	2	2
Lacrimal gland	1	1	1
Accessory lacrimal gland	1	1-2	1

OARs: organs at risk, PRV: planning organ at risk volume.

shifts performed for actual treatment after CBCTs had been compared with the reference planning CT images. We described a PRV in the dorsoventral, mediolateral, and craniocaudal axis for the ocular globe, ocular lens, optic nerve, optic chiasm, retina, cornea, lacrimal gland, and accessory lacrimal gland based on 30 dogs.

Contouring of some ocular structures proved to be difficult, even on diagnostic contrast-enhanced CT images. Transition between retina and cornea is not easily visible even on diagnostic contrast-enhanced images and was therefore performed subjectively. To simplify contouring and due to limitations of the contouring tools and visibility on CT images, the retina and cornea were contoured outside the globe as described above. This could have impacted the volume measurements, and may have influenced the PRV estimates. Accessory lacrimal glands were not visible on unenhanced CBCTs and helper structures including adjacent bone were used. This did not account for third eyelid movement and made location dependent on bone and therefore positioning errors and might therefore have underestimated true shifts. Magnetic resonance imaging has been suggested for better identifying the optic nerve but was not available for this population of dogs.[29,30]

Knowing the possible positions of the OARs during a treatment course facilitates planning and sparing of OARs. This is especially important when considering new simultaneously-integrated boost treatments or stereotactic body radiation therapy as is emerging in veterinary radiation oncology and sinonasal irradiation at present.[9,24,25,27,31] A comparison of plans with and without PRV in human nasal cavity and paranasal cancer patients showed equal target dose coverage but a significant decrease in ocular OAR dose with help of ocular PRVs.[15]

The PRV expansions in our study were very small in the majority of OARs and directions with the exception of the ocular lens, optic nerve, retina, and cornea. The ocular globe, and therefore the lens, retina, and cornea can rotate, most likely explaining the larger PRV expansions. This movement can for example change with depth of anesthesia; however, this was not specifically assessed in the present study.[5] Table 2 shows rounded PRV expansion margins for easier clinical use. We included a range where applying mathematical rounding would have led to a lower number, despite being rather in-between two numbers (i.e. 1–2 mm for the ocular globe for a value of 1.321 mm) as more conservative (less risky) approach. With this range the reader can decide if use of the smaller expansion margin (eg, if PTV and PRV are overlapping) or rather use of the "safer," larger expansion margin (eg, if PTV and PRV are wide apart) is more appropriate. Because we included only one brachycephalic dog in our sample, it is possible that our margin estimates may not be generalizable for brachycephalic breeds.

The PRV should not be mistaken for the true daily position of the OAR as it considers different possible positions over a whole course of treatment. Our study retrospectively looked at datasets with daily imaging. However, only orthogonal kV radiographs were performed daily; CBCT was performed at least four times during a course of treatment (i.e. for approximately every second to third fraction) and not daily due to the retrospective nature of the study. Those CBCTs were assumed to represent the possible shifts during the whole course of treatment due to the rigid maxillary dental mold and daily kV-kV imaging with bone alignment; however, daily CBCT-imaging would have been needed to verify this. While a PRV should influence treatment planning and guide shaping of dose distribution, it should not lead to target volume underdosage due to its inherent uncertainties. Underdosage of target volumes most likely leads to inferior tumor control

as shown by tumor control probability models.[32,33] Increasing accuracy/precision of patient positioning with resulting smaller target volumes has therefore utmost priority, as OARs in close vicinity can be spared with advanced techniques and sharp dose fall-off.[4,34]

A PRV of the lens has already been established in dogs.[6] The lens is exclusively sensitive already to low doses of radiation and cataract formation can lead to loss of vision.[2,35] Cataract formation is, however, a non-life-threatening disease and can be treated with phacoemulsification surgery to restore vision.[36] Other ocular and periocular organs can be subject to radiation-induced damage: keratitis, keratoconjunctivitis sicca, retinal hemorrhage or glaucoma can occur and impair quality of life or lead to vision impairment.[2,37,38] Establishing a PRV not only for the lens, but also for other periocular and ocular structures is an important step towards future research including establishment of tolerance doses.

In contrast to the study of Jafry et al, we decided to report our PRV margins as individual expansion margins in each axis in each OAR.[6] This considers the directional shifts that are more pronounced in one or two directions in some OARs, as shown for example in corneas and retinas. Jafry et al used a similar rigid positioning device and reported a 3 mm PRV expansion margin for the ocular lens. This is larger than our proposed conservative estimate of 2 mm. It is important to point out that – although similar – positioning devices might differ between institutions. Jafry et al also performed new co-registrations with bone alignment at the level of the eyes and brain and did not use online registration previously used for treatment of the dogs, thereby eliminating interobserver variability. Our approach more closely resembles daily clinical routine: staff might change during a course of treatment or alignment might be performed depending on the location of the tumor (eg, rostral vs caudal). A prudent PRV of 2-3 mm might be considered for the ocular lens in dogs for the future.

Different limitations should be addressed. The majority of dogs included in our study underwent RT with 10 fractions, were daily matched with orthogonal kV-imaging but only had four positioning verifications with CBCT over the course of treatment. For fractions with 2D orthogonal positioning verification only, roll displacements might not have been displayed correctly.[39] Looking at occasional 3D images (CBCTs) only for matching might therefore not represent the true OAR displacement during the whole course of treatment (ie, all 10 fractions). The shifts detected could therefore be an under- or overestimate of the true daily shifts. In addition, with our equipment, displacements with submillimeter accuracy or rotational errors (roll, pitch) were not corrected due to on-board imager with 1 mm precision and a four degrees-of-freedom couch. A six degrees-of-freedom couch would change ocular PRVs. However, not all human and only few veterinary facilities report the use of image-guidance with a six degree-of-freedom couch able to correct roll and pitch and achieving ≤0.5 mm positioning accuracy. Currently there is an ongoing controversial discussion in human radiation oncology whether a six degree-of-freedom couch is necessary for all patients or is for example only clinically beneficial and therefore indicated for certain patients, such as for stereotactic radiotherapy protocols.[40,41] Another limitation was that the quality of CT images could have been affected by outside variables (eg, slice thickness, field of view). In order to import CT images into the treatment planning system, a reconstruction for RT is performed and might include larger slice thickness, thereby decreasing visibility of small ocular OAR and contouring accuracy. CBCT quality is inferior to a diagnostic helical CT scan, and contrast agent highlighting certain structures is not routinely administered for position verification.[42,43] This was demonstrated by both the accessory and lacrimal glands being invisible on the CBCTs in our study. Also, the ocular globes were of different volume if contoured from scratch on the CBCT due to inferior visibility. We therefore created helper structures that either helped maintain the volume of the OAR that should not change in between fractions (as in the ocular globe) or helped localize the OAR. Another limitation was that some OARs were difficult to contour. For example, MRI would have been needed for more consistent delineation of the optic chiasm. This likely influenced the size of optic chiasm PRV estimates. Another limitation was that the same observer performed all measurements, therefore interobserver variability was not assessed. Previous studies demonstrated marked target volume and OAR contouring variations between different human and veterinary radiation oncologists.[44–46] These variations could also influence PRVs. Human radiation oncologists circumvented the lack of comprehensive identification and delineation of OARs by a standardized delineation guide.[47] Such a standardized system would be of great advantage for veterinary radiation oncologists in the future. Interobserver variability was minimized in our study by all contours being delineated by one of the authors (FW) and checked by a veterinary radiation oncologist (VM) as mentioned above. Another limitation was that the original treatment plans were selected and performed by varying radiation oncologists. Contouring is not the only step in RT that can vary between individuals, also the imaging matching process for positioning of patients can be different between different radiation therapists or oncologists and depends on their experience.[48] For a canine sinonasal tumor this could mean putting emphasis on a perfect imaging match in the region of the eye ipsilateral to the tumor or with emphasis on a match in the region of the olfactory bulb or there could be a balance between the two different possible matching points. Because our PRV was established from retrospective data, it was not possible to determine the location of the most exact match.

In conclusion, the ocular PRV estimates described in this study – with aid of a rigid positioning system and 3D-image guidance – may help improve awareness of and minimization of dose in (peri-)ocular OARs for future patients. Due to the limitations mentioned above, PRV estimates need to be implemented with caution and adapted to each institution's equipment. It remains to be elucidated if PRVs will lead to a measurable decrease in clinical ocular radiation toxicity in the future.

LIST OF AUTHOR CONTRIBUTIONS

Category 1

(a) Conception and Design: Wolf, Rohrer Bley, Besserer, Meier
(b) Acquisition of Data: Wolf, Meier
(c) Analysis and Interpretation of Data: Rohrer Bley, Besserer, Meier

Category 2

(a) Drafting the Article: Wolf, Rohrer Bley, Meier
(b) Revision Article for Intellectual Content: Wolf, Rohrer Bley, Besserer, Meier

Category 3

(a) Final Approval of the Complete Article: Wolf, Rohrer Bley, Besserer, Meier

DATA AVAILABILITY STATEMENT

The data that support the findings of this study are openly available in Harvard Dataverse at https://doi.org/10.7910/DVN/B4ID7M, reference number UNF:6rMz1V7mRJT89Od3uMDKIrQ = = [fileUNF].

ACKNOWLEDGEMENTS

This work was supported by the Swiss National Science Foundation (SNSF), grant number: 320030-182490; PI: Carla Rohrer Bley.

CONFLICT OF INTEREST

The authors declare no conflict of interest.

ORCID

Carla Rohrer Bley https://orcid.org/0000-0002-5733-2722
Valeria Meier https://orcid.org/0000-0003-0793-9005

REFERENCES

1. *International Commission on Radiation Units and Measurements*. Prescribing, Recording, and Reporting Photon Beam Therapy (Report 62, Supplement to ICRU Report 50). Bethesda, MD, 1999. https://icru.org/home/reports/prescribing-recording-and-reporting-photon-beam-therapy-report-62.
2. Wolf F, Meier VS, Pot SA, Rohrer Bley C. Ocular and periocular radiation toxicity in dogs treated for sinonasal tumors: a critical review. *Vet Ophthalmol*. 2020;23:596-610.
3. Askoxylakis V, Hegenbarth P, Timke C, Saleh-Ebrahimi L, Debus J, Roder F. Intensity modulated radiation therapy (IMRT) for sinonasal tumors: a single center long-term clinical analysis. *Radiat Oncol (London, England)*. 2016;11:17.
4. Lawrence JA, Forrest LJ, Turek MM, Miller PE, Mackie TR, Jaradat HA. Proof of principle of ocular sparing in dogs with sinonasal tumors treated with intensity-modulated radiation therapy. *Vet Radiol Ultrasound*. 2010;51:561-570.
5. Costa D, Leiva M, Moll X, Aguilar A, Pena T, Andaluz A. Alfaxalone versus propofol in dogs: a randomised trial to assess effects on peri-induction tear production, intraocular pressure and globe position. *Vet Rec*. 2015;176:73.
6. Jafry Z, Gal A, Fleck A, Darko J, Poirier VJ. Proposed expansion margins for planning organ at risk volume for lenses during radiation therapy of the nasal cavity in dogs and cats. *Vet Radiol Ultrasound*. 2017;58:471-478.
7. McKenzie A, van Herk M, Mijnheer B. Margins for geometric uncertainty around organs at risk in radiotherapy. *Radiother Oncol*. 2002;62:299-307.
8. van Herk M, Remeijer P, Rasch C, Lebesque JV. The probability of correct target dosage: dose-population histograms for deriving treatment margins in radiotherapy. *Int J Radiat Oncol Biol Phys*. 2000;47:1121-1135.
9. Soukup A, Meier V, Pot S, Voelter K, Rohrer Bley C. A prospective pilot study on early toxicity from a simultaneously integrated boost technique for canine sinonasal tumours using image-guided intensity-modulated radiation therapy. *Vet Comp Oncol*. 2018;16:441-449.
10. Zwingenberger AL, Park SA, Murphy CJ. Computed tomographic imaging characteristics of the normal canine lacrimal glands. *BMC veterinary research*. 2014;10:116.
11. Evans HE, De Lahunta A. *Miller's anatomy of the dog*. Elsevier; 2012.
12. Rossi F, Korner M, Suarez J, Carozzi G, Meier VS, Roos M. Computed tomographic-lymphography as a complementary technique for lymph node staging in dogs with malignant tumors of various sites. *Vet Radiol Ultrasound*. 2018;59:155-162.
13. Quality assurance of gantry-mounted image-guided radiotherapy systems. http://www.ssrpm.ch/old/recrep-m.htm#rec:: Swiss Society of Radiobiology and Medical Physics, 2010;1-16.
14. Gregoire V, Mackie TR. State of the art on dose prescription, reporting and recording in Intensity-Modulated Radiation Therapy (ICRU report No. 83). *Cancer Radiother*. 2011;15:555-559.
15. Piotrowski T, Ryczkowski A, Adamczyk M, Jodda A. Estimation of the planning organ at risk volume for the lenses during radiation therapy for nasal cavity and paranasal sinus cancer. *J Med Imaging Radiat Oncol*. 2015;59:743-750.
16. Zou W, Dong L, Kevin Teo BK. Current state of image guidance in radiation oncology: implications for PTV margin expansion and adaptive therapy. *Semin Radiat Oncol*. 2018;28:238-247.
17. Den RB, Doemer A, Kubicek G, Bednarz G, Galvin JM, Keane WM. Daily image guidance with cone-beam computed tomography for head-and-neck cancer intensity-modulated radiotherapy: a prospective study. *Int J Radiat Oncol Biol Phys*. 2010;76:1353-1359.
18. Maund IF, Benson RJ, Fairfoul J, Cook J, Huddart R, Poynter A. Image-guided radiotherapy of the prostate using daily CBCT: the feasibility and likely benefit of implementing a margin reduction. *Br J Radiol*. 2014;87:20140459.
19. Gupta M, Gamre P, Kannan S, Rokde G, Krishnatry R, Murthy V. Effect of imaging frequency on PTV margins and geographical miss during image guided radiation therapy for prostate cancer. *Pract Radiat Oncol*. 2018;8:e41-e47.
20. Morimoto CY, Mayer MN, Sidhu N, Bloomfield R, Waldner CL. Setup error with and without image guidance using two canine intracranial positioning systems for radiation therapy. *Vet Comp Oncol*. 2020.
21. Feng Y, Lawrence J, Cheng K, Montgomery D, Forrest L, McLaren DB. Invited review - Image registration in veterinary radiation oncology: indications, implications, and future advances. *Vet Radiol Ultrasound*. 2016;57:113-123.
22. Kubicek LN, Seo S, Chappell RJ, Jeraj R, Forrest LJ. Helical tomotherapy setup variations in canine nasal tumor patients immobilized with a bite block. *Vet Radiol Ultrasound*. 2012;53:474-481.
23. Deveau MA, Gutierrez AN, Mackie TR, Tome WA, Forrest LJ. Dosimetric impact of daily setup variations during treatment of canine nasal tumors using intensity-modulated radiation therapy. *Vet Radiol Ultrasound*. 2010;51:90-96.
24. Kubicek L, Milner R, An Q, Kow K, Chang M, Cooke K. Outcomes and prognostic factors associated with canine sinonasal tumors treated with curative intent cone-based stereotactic radiosurgery (1999-2013). *Vet Radiol Ultrasound*. 2016;57:331-340.
25. Glasser SA, Charney S, Dervisis NG, Witten MR, Ettinger S, Berg J. Use of an image-guided robotic radiosurgery system for the treatment of canine nonlymphomatous nasal tumors. *J Am Anim Hosp Assoc*. 2014;50:96-104.
26. LaRue SM, Custis JT. Advances in veterinary radiation therapy: targeting tumors and improving patient comfort. *Vet Clin North Am Small Anim Pract*. 2014;44:909-923.

27. Nolan MW, Gieger TL. Update in veterinary radiation oncology: focus on stereotactic radiation therapy. *Vet Clin North Am Small Anim Pract*. 2019;49:933-947.
28. Meduri B, Gregucci F, D'Angelo E, Alitto AR, Ciurlia E, Desideri I. Volume de-escalation in radiation therapy: state of the art and new perspectives. *J Cancer Res Clin Oncol*. 2020;146:909-924.
29. Eekers DB, In 't Ven L, Roelofs E, Postma A, Alapetite C, Burnet NG. The EPTN consensus-based atlas for CT- and MR-based contouring in neuro-oncology. *Radiother Oncol*. 2018;128:37-43.
30. Boroffka SA, Gorig C, Auriemma E, Passon-Vastenburg MH, Voorhout G, Barthez PY. Magnetic resonance imaging of the canine optic nerve. *Vet Radiol Ultrasound*. 2008;49:540-544.
31. Dunfield EM, Turek MM, Buhr KA, Christensen NI. A survey of stereotactic radiation therapy in veterinary medicine. *Vet Radiol Ultrasound*. 2018;59:786-795.
32. Goitein M. *Biology matters*. Radiation oncology: a physicist's-eye view. New York, USA: Springer; 2010:85-110.
33. Tsien C, Eisbruch A, McShan D, Kessler M, Marsh R, Fraass B. Intensity-modulated radiation therapy (IMRT) for locally advanced paranasal sinus tumors: incorporating clinical decisions in the optimization process. *Int J Radiat Oncol Biol Phys*. 2003;55:776-784.
34. Hansen KS, Theon AP, Dieterich S, Kent MS. Validation of an Indexed Radiotherapy Head Positioning Device for Use in Dogs and Cats. *Vet Radiol Ultrasound*. 2015;56:448-455.
35. Hamada N, Azizova TV, Little MP. An update on effects of ionizing radiation exposure on the eye. *Br J Radiol*. 2019:20190829.
36. Krishnan H, Hetzel S, McLellan GJ, Bentley E. Comparison of outcomes in cataractous eyes of dogs undergoing phacoemulsification versus eyes not undergoing surgery. *Vet Ophthalmol*. 2020;23:286-291.
37. Ching SV, Gillette SM, Powers BE, Roberts SM, Gillette EL, Withrow SJ. Radiation-induced ocular injury in the dog: a histological study. *Int J Radiat Oncol Biol Phys*. 1990;19:321-328.
38. Roberts SM, Lavach JD, Severin GA, Withrow SJ, Gillette EL. Ophthalmic complications following megavoltage irradiation of the nasal and paranasal cavities in dogs. *J Am Vet Med Assoc*. 1987;190:43-47.
39. Magestro LM, Cahoon JY, Gieger TL, Nolan MW. Radiotherapy isocenters verified by matching to bony landmarks of the canine and feline head differ when localized using volumetric versus planar imaging. *Vet Comp Oncol*. 2019;17:562-569.
40. Njeh CF, Snyder KC, Cai J. The use of six degrees of freedom couch is only clinically beneficial in stereotactic radio surgery. *Med Phys*. 2019;46:415-418.
41. Stieb S, Malla M, Graydon S, Riesterer O, Klock S, Studer G. Dosimetric influence of pitch in patient positioning for radiotherapy of long treatment volumes; the usefulness of six degree of freedom couch. *Br J Radiol*. 2018;91:20170704.
42. Siewerdsen JH, Jaffray DA. Cone-beam computed tomography with a flat-panel imager: magnitude and effects of x-ray scatter. *Med Phys*. 2001;28:220-231.
43. Xu Y, Bai T, Yan H, Ouyang L, Pompos A, Wang J. A practical cone-beam CT scatter correction method with optimized Monte Carlo simulations for image-guided radiation therapy. *Phys Med Biol*. 2015;60:3567-3587.
44. Riegel AC, Vaccarelli M, Cox BW, Chou H, Cao Y, Potters L. Impact of Multi-Institutional Prospective Peer Review on Target and Organ-at-Risk Delineation in Radiation Therapy. *Practical radiation oncology*. 2019;9:e228-e235.
45. Huo M, Gorayski P, Poulsen M, Thompson K, Pinkham MB. Evidence-based Peer Review for Radiation Therapy - Updated Review of the Literature with a Focus on Tumour Subsite and Treatment Modality. *Clin Oncol (R Coll Radiol)*. 2017;29:680-688.
46. Christensen NI, Forrest LJ, White PJ, Henzler M, Turek MM. Single institution variability in intensity modulated radiation target delineation for canine nasal neoplasia. *Vet Radiol Ultrasound*. 2016;57:639-645.
47. Wright JL, Yom SS, Awan MJ, Dawes S, Fischer-Valuck B, Kudner R, et al. Standardizing Normal Tissue Contouring for Radiation Therapy Treatment Planning: an ASTRO Consensus Paper. *Pract Radiat Oncol*. 2019;9:65-72.
48. Cooper D, Saberi M, Galiano E. An analysis of inter-operator registration variability in helical tomotherapy. *J Med Imaging Radiat Sci*. 2008;39:135-143.

SUPPORTING INFORMATION

Additional supporting information may be found online in the Supporting Information section at the end of the article.

How to cite this article: Wolf F, Rohrer Bley C, Besserer J, Meier V. Estimation of planning organ at risk volumes for ocular structures in dogs undergoing three-dimensional image-guided periocular radiotherapy with rigid bite block immobilization. *Vet Radiol Ultrasound*. 2021;62:246–254. https://doi.org/10.1111/vru.12955